

The performance of TiO₂/NaY-zeolite nanocomposite in photocatalytic degradation of Microcystin-LR from aqueous solutions: Optimization by response surface methodology (RSM)

Afshin Ebrahimi¹, Negar Jafari¹, Karim Ebrahimpour¹, Ali Nikoonahad², Amir Mohammadi³, Farzad Fanaei⁴, Ali Abdollahnejad³

¹Department of Environmental Health Engineering, School of Health, Isfahan University of Medical Sciences, Isfahan, Iran

²Department of Environmental Health Engineering, Faculty of Health, Ilam University of Medical Sciences, Ilam, Iran

³Department of Public Health, Maragheh University of Medical Sciences, Maragheh, Iran

⁴Department of Environmental Health Engineering, Faculty of Health, Iran University of Medical Sciences, Tehran, Iran

Abstract

Background: Microcystin (MC) is a hepatotoxic and carcinogenic toxin that is generated by cyanotoxins which can have adverse effects on the human health. Therefore, it is very important to remove it from the environment. This study was performed to investigate the efficiency of titanium dioxide (TiO₂)/NaY-zeolite (T/N-Z) nanocomposite for removal of MC-LR under ultraviolet light.

Methods: In the present study, T/N-Z nanocomposite was synthesized using the hydrothermal method. Specification of the photocatalysts was determined by the field emission scanning electron microscopy (FESEM), X-ray diffraction (XRD), and Fourier transform infrared spectroscopy (FT-IR) spectra. The response surface methodology (RSM) was used to survey the effects of operating variables such as pH, contact time, and catalyst dose on the removal of MC-LR. The MC-LR concentration was measured by high-performance liquid chromatography (HPLC).

Results: It was revealed that the increase of contact time and catalyst dose had a positive effect on enhancing the removal efficiency of MC-LR, but pH had a negative effect. Finally, the maximum MC-LR removal efficiency was 97.63%, which occurred at pH = 5, contact time = 120 min, and catalyst dose = 1.2 g/L.

Conclusion: In general, T/N-Z composite in aqueous solutions under the UV light can easily decompose MC-LR and it can also be proposed as an efficient composite for removal of MC-LR from contaminated water.

Keywords: Microcystin, Titanium dioxide, Zeolite, Photocatalytic degradation, High-performance liquid chromatography

Citation: Ebrahimi A, Jafari N, Ebrahimpour K, Nikoonahad A, Mohammadi A, Fanaei F, Abdollahnejad A. The performance of TiO₂/NaY-zeolite nanocomposite in photocatalytic degradation of Microcystin-LR from aqueous solutions: Optimization by response surface methodology (RSM). *Environmental Health Engineering and Management Journal* 2020; 7(4): 245-256. doi: 10.34172/EHEM.2020.29.

Article History:

Received: 28 July 2020

Accepted: 11 December 2020

ePublished: 22 November 2020

*Correspondence to:

Negar Jafari,

Email: n64jafari@gmail.com

Ali Abdollahnejad, Email:

abdollahnejad.a@gmail.com

Introduction

Various chemical toxins are produced by cyanobacteria (blue-green algae) which can be hazardous to the human health and the environment (1). Ecological disruptions associated with rising urbanization, agricultural activities, and climate changes have increased the intensity, frequency, and geographic distribution of cyanobacteria (2). One of the most important cyanotoxins produced with a widespread distribution is microcystin (MC) that is a class of biologically active cyclic heptapeptide compounds, with over 100 known variants, and in most

studies related to water treatment, is considered as an indicator (3). Toxins produced by cyanobacteria include hepatotoxins, neurotoxins, cytotoxins, dermatotoxins, and gastrointestinal toxins that threaten the human public health and the environment (4,5). MCs are the most well-known family of cyanotoxin that are found in rivers and lakes and water reservoirs (6). MC is water-soluble, heat-resistant, and has a strong toxicity that cannot be removed by boiling at a high temperature (7). After being absorbed by flora and fauna, this toxin is transferred to the human body via the food chain and is widely distributed



in water, and thus, endangers the ocean ecology (8). MC-LR is a hepatotoxic cyanotoxin that acute and chronic exposure to this toxin in addition to liver cancer in human beings can have harmful effects on the kidney, heart, and the gastrointestinal tract (9). Therefore, it is the most important threat to drinking water (10). Because of the potent toxicity, the International Agency for Research on Cancer (IARC) has categorized MC-LR as possibly carcinogenic to humans (Group 2B). And the guideline value set by the World Health Organization (WHO) for MC-LR in drinking water is 1 µg/L (11). So, the removal of MC-LR from drinking water resources is very necessary for human health and environmental safety (12). Various techniques have been suggested for the cyanobacteria cells and MCs control in drinking water, such as coagulation, flocculation, filtration, activated carbon, membrane filtration, oxidation processes etc (13). However, the traditional water treatment systems can remove only cyanobacterial cells while having limited capability to remove cyanotoxins and is associated with different practical, economic or environmental disadvantages (14,15). On the other hand, the traditional treatment processes may cause the release of cyanotoxins into the water by ripping the cyanobacterial cells, and potentially increase the risk of secondary pollution (16). Removal of extracellular MC by microfiltration and ultrafiltration techniques is not an effective method because it requires costly pumping of water (17). The nanofiltration and reverse osmosis membranes reduced MC-LR more than 95% but they require a high cost. Recently, advanced oxidation processes (AOPs) such as the photocatalytic oxidation process due to its efficiency in decomposition and mineralization of resistant compounds such as cyanotoxins have received significant attention (18). Numerous studies have confirmed the removal of MC-LR by the AOPs (19). In the studies of Pelaez et al and Zhang et al, the photocatalytic degradation of MC-LR by N-F-codoped titanium dioxide (TiO₂) and S-N-C codoped TiO₂ processes, respectively, was investigated. They found that these photocatalysts were highly efficient in the removal of MC-LR (12,20). Also, the study of Yang et al showed that the rate of MC-LR degradation using TiO₂ (0.05 g L⁻¹) in 15 minutes reached 99.9% (21). Advanced oxidation methods such as TiO₂ photocatalysis have well confirmed the removal of MCs (22). TiO₂ catalyst by absorbing photons, transfers photoexcited electrons (e⁻) from the valence band (VB) to conduction band (CB), and subsequently, creates holes in the VB (h⁺) that lead to the formation of e⁻/h⁺ pairs. Next, the photogenerated electrons in the CB react with O₂ for the generation of [•]O₂⁻ radicals and photogenerated holes in the VB react with H₂O molecules for the generation of [•]OH radicals (23,24). Finally, the active radicals attack the C₄-C₅ and C₆-C₇ unsaturated double bonds (active sites for reaction) in the Adda side-chain, resulting in the hydroxylation of MC-LR and formation of aldehyde and ketone derivatives (9,25).

Among the AOPs, TiO₂ as a semiconductor material is able to effectively decompose water contaminations due to its favorable properties such as high chemical and thermal stabilities, nontoxicity, commercial availability, and low cost (26).

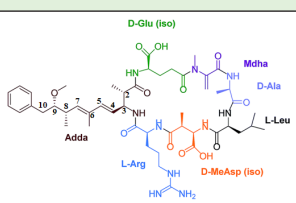
In last years, many studies have been performed to modify the TiO₂ structure with metallic or non-metallic compounds to increase the stability and efficiency of TiO₂ (27-29). For example, numerous studies have been performed on the use of the combination of TiO₂ with Bi-based semiconductors such as Bi-TiO₂ (30) and bismuth oxyhalides (BiOXs, X = Cl, Br, I) (31) or the combination of TiO₂ with metallic compounds such as Ag/AgCl/TiO₂ (23), or graphene-TiO₂ (9) and CdS/B-TiO₂ (29) for photocatalytic degradation of MC-LR. Also, the combination of TiO₂ with zeolite has been used for removal of various pollutants such as VOCs, ibuprofen, sulfadiazine, and benzene, which has shown favorable results (28,32,33). However, no study has been conducted to investigate the effect of the combination of TiO₂/zeolite on removal of MC-LR. Therefore, the present study was performed to synthesize a composite with coating of TiO₂ on the zeolite surface as a low-cost material to increase the removal efficiency of MC-LR. Response surface methodology (RSM) is a statistical and experimental strategy to get the optimum conditions for a multivariable system and it has been successfully applied to different photocatalytic processes for achieving its optimization using experimental designs. RSM is a suitable strategy which can improve a system and enhance the efficiency of the process without increasing the cost (34,35). So, in this study, in order to determine the optimum conditions for MC-LR removal by the TiO₂/NaY-zeolite (T/N-Z) nanocomposite under UV light, RSM based on the central composite design (CCD) was used.

Materials and Methods

Materials

The standard solution of MC-LR (10 µg/mL) and standard powder (100 µg) was purchased from Sigma-Aldrich Company (Germany). Also, titanium dioxide (TiO₂ anatase with purity of 99.9%, particle size of 20 nm, and BET >200 m²/g) was purchased from Sigma-Aldrich Company (Germany). The standard solutions were prepared by dissolving 100 µg standard powder of MC-LR in 1 mL of methanol (100%), then, diluted with distilled water with purity of 99% (Merck Co., Germany) and experiment solutions were prepared. All solutions were stored at -20 C until use. NaY-zeolite was purchased from Pioneers Clean Environment Company (Iran). Other chemical materials such as methanol, acetonitrile, trifluoroacetic acid (TFA) (HPLC-grade), sodium hydroxide, and hydrochloric acid were purchased from Merck Company (Germany). Properties of MC-LR are presented in Table 1.

Table 1. Properties of MC-LR (MC-LR)

Molecular Properties	MC-LR
Structure	
Formula	$C_{49}H_{74}N_{10}O_{12}$
Weight	995.2 g/mol

Synthesis of TiO₂/NaY-zeolite nanocomposite

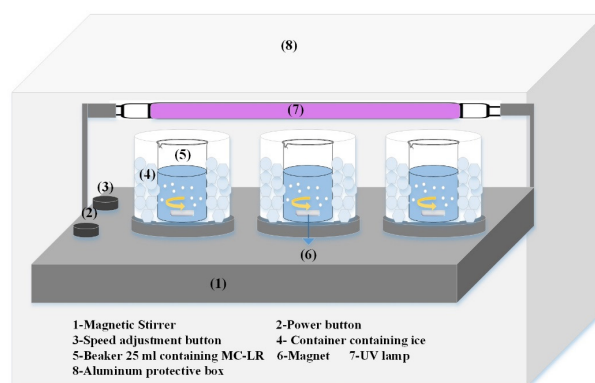
The T/N-Z nanocomposite was synthesized using the hydrothermal method. For this purpose, first 0.5 g of TiO₂ and 1.2 g of NaY-zeolite were dissolved in 50 mL of ethanol, then, the white solution created was placed in an ultrasonic bath for 0.5 hours. In the next step, in order to evaporate and remove the ethanol, the solution was stirred and the remaining sample at the bottom of the container was collected using a filter paper and washed with distilled water several times and dried at 110 °C for 8 hours. In the final step, for calcining the nanocomposite, the sample was transferred into a furnace at 500 °C for 6 hours (36). Finally, the prepared nanocomposite was used for the experiments.

Characterization study

To investigate the structure and surface morphology of TiO₂ nanoparticles, the field emission scanning electron microscopy (FESEM) (FEI Quanta 200, USA) and X-ray diffractometer (Bruker D8 ADVANCE, Germany) were used. Also, the FTIR spectrum of TiO₂/NaY-zeolite was studied by an IR spectrometer (Jasco 6300, Japan).

Photocatalytic study

All of the experiments were conducted using a catalyst mixture and 10 mL of aquatic solutions was mixed with 500 µg/L MC-LR in 25 mL Pyrex beakers, which was inside a container containing ice (Figure 1). For adjusting the samples pH, NaOH (0.01 M) and HCl were used. To eliminate the aggregates, the samples were placed in an ultrasonic bath (10 minutes). A 100 W mercury lamps (wavelength of 254 nm) were placed 10 cm above Pyrex beakers. Before illumination, the samples were stirred for 30 min in darkness to reach the equilibrium of adsorption and desorption between the photocatalyst and MC-LR. Then, UV lamps were turned on, and the samples were located under magnetic stirring to keep the uniformity of the suspension. At the end of the contact time, UV lamps were turned off and the samples were derived. Before injecting the samples into HPLC for measurement of the MC-LR residual concentration, catalyst particles were separated from the samples using syringe filters (0.22 µm).

**Figure 1.** Schematic diagram of the experimental setup for the MC-LR degradation.

Design of experiments and optimization

In this study, RSM was used to optimize the number of experiments and to assess the interactive effects of the significant operating parameters in the degradation of MC-LR by T/N-Z nanocomposite using the Design-Expert software version 10 (37,38). According to the CCD, three variables including pH (A), contact time (B), and catalyst dose (C) were selected as model variables (Table 2).

Eventually, 20 different experimental runs were designed that along with the actual and predicted values of MC-LR removal are shown in Table 3. The coded values of independent variables were calculated using Eq. (1):

$$X_i = \frac{(X_i - X_0)}{\Delta X} \quad (1)$$

Where X_i is the coded value of the independent variable, X_0 is the center point value, and ΔX is the change value (39). To survey the interaction between the independent and dependent variables in the number of the runs, the regression model was used as Eq. (2):

$$Y = \beta_0 + \sum \beta_i X_i + \sum \beta_{ii} X_i^2 + \sum \beta_{ij} X_i X_j \quad (2)$$

Where Y is the predicted value of MC-LR removal, β_0 is the model constant, β_i is the linear coefficient, β_{ii} is the coefficient of quadratic factor, and the β_{ij} is the cross product coefficient.

Analytical methods

The residual concentration of MC-LR was measured using HPLC (Jasco PU-2080, Tokyo, Japan) equipped with

Table 2. Actual and coded values of independent variables using central composite design (CCD)

Variables	Unit	Symbols	Actual values of the coded values				
			-2	-1	0	+1	+2
pH (A)	-	A	4	5	7	9	10
Contact time (B)	min	B	6	30	75	120	144
Catalyst dose (C)	g/L	C	0.44	0.6	0.9	1.2	1.35

Table 3. Experimental design conditions and responses of various experimental runs

Run No.	A: pH	Variables		MC-LR removal (%)	
		B: Contact time (min)	C: Catalyst dose (g/L)	Actual	Predicted
1	7	75	0.9	89.53	88.39
2	7	143.60	0.9	91.8	90.10
3	7	75	0.9	87.95	88.39
4	10	75	0.9	80.44	79.82
5	7	75	0.9	89.12	88.39
6	7	75	0.44	82.4	82.07
7	5	120	1.2	97.63	97.97
8	5	30	1.2	93.36	92.36
9	9	120	1.2	85.27	86.00
10	9	30	0.6	77.4	77.09
11	7	75	1.36	92.16	92.45
12	5	30	0.6	84.96	84.26
13	9	120	0.6	79.47	80.49
14	9	30	1.2	84.22	83.73
15	7	6.39	0.9	81.59	83.24
16	4	75	0.9	93.83	94.40
17	7	75	0.9	87.89	88.39
18	7	75	0.9	87.58	88.39
19	5	120	0.6	90.47	90.99
20	7	75	0.9	88.23	88.39

a quaternary mixing pump, an in-line vacuum degasser, a UV-Vis detector (UV-2075 plus), and an auto-injector (AS-2055 Plus). Samples were separated by the C_{18} column (150 × 4.6 mm, 5 μm particles). The combination of acetonitrile and Milli-Q water with a volume ratio of 50:50 with 0.1% Trifluoroacetic acid (TFA) was used as a mobile phase with a flow rate of 1 mL/min. Due to the typical absorption spectra of MC-LR, the wavelength of the UV detector was set at 238 nm. The injection volume was 100 μL with a flow rate of 1 mL/min and the total run time was 15 minutes. Borwin chromatography software (version 1.50) was used for data acquisition and processing HPLC. The degradation rate of MC-LR was determined by Eq. (3):

$$\text{Degradation rate (\%)} = C_0 - C/C_0 * 100 \quad (3)$$

Where C_0 and C are the initial and residual concentrations of MCLR, respectively.

To determine the point of zero charge of T/N-Z nanocomposite, 0.2 g nanocomposite was added to 50 mL of NaCl solution (0.1 M). HCl or NaOH solutions were used for pH adjustment. The solution was then mixed on a shaker at 150 rpm at room temperature for 48 h. Eventually, the final pH of the solution was measured by a pH meter (EUTECH 310) (40).

Analytical method validation

To validate the analytical method of MC-LR by HPLC, relative recovery, limit of detection (LOD), and limit of

quantification (LOQ) were calculated according to the recommendations of the International Conference on Harmonization (Table 4).

Results

Characterization study

FE-SEM analysis

The FESEM images of NaY-zeolite, and TiO_2 semiconductors, and T/N-Z nanocomposite are presented in Figure 2a-c. Figure 2a shows that NaY-zeolite was in the form of cubic and polyhedral crystals and the size of these particles was about 100 to 600 nm. Figure 2b represents the FESEM image of the TiO_2 nanoparticles. According to this figure, the size of TiO_2 nanoparticles which have spherical and dense shapes, was about 20 nm. The FESEM image of T/N-Z nanocomposite in Figure 2c shows that TiO_2 and NaY-zeolite nanoparticles overlapped well and formed a homogeneous nanocomposite.

XRD analysis

The crystalline phase of and XRD patterns of NaY-zeolite, TiO_2 , and T/N-Z nanocomposite are shown in Figure 3. As shown in this figure, all the recognized peaks of NaY-

Table 4. Analytical method validation parameters for determination of MC-LR by HPLC

Parameter	Recovery (%)	LOD (μg/L)	LOQ (μg/L)
MC-LR	102 ± 9.5	4.04	12.24

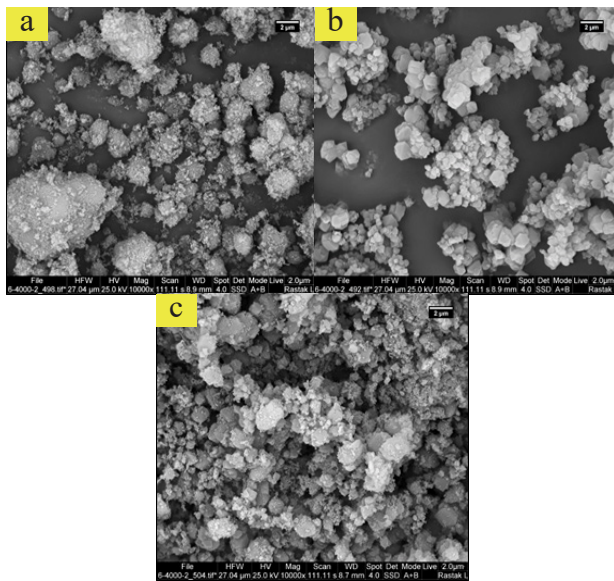


Figure 2. The FE-SEM images of NaY-zeolite (a), TiO₂ (b), T/N-Z nanocomposite (c).

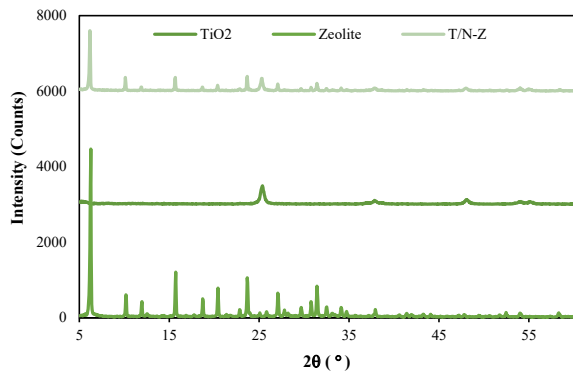


Figure 3. The XRD patterns of NaY-zeolite, TiO₂, and T/N-Z nanocomposite.

zeolite (Na₅Al₆Si₃₀O₇₂ · 18H₂O formula) showed distinct diffraction peaks at 2θ of 6.22°, 10.16°, 15.68°, 23.66°, and 31.42°, which was corresponded to the crystal phase of NaY-zeolite (JCPDS PDF No. 43-0168) (28,41). The XRD patterns of the TiO₂ (anatase) sample are shown in Figure 3. Six strong diffraction peaks of TiO₂ were observed at 2θ values of 25.55°, 38.1°, 47.95°, 54.15°, 55.65°, and 62.52°, which were consistent with (101), (004), (200), (211), and (204) crystallographic plane of TiO₂ anatase phases (JCPDS No. 21-1272) (42). The XRD pattern of the synthesized T/N-Z nanocomposite shows obvious peaks at 2θ of 6.22°, 15.55°, 23.5°, 27.23°, and 30.5°, which were corresponded to the NaY-zeolite phase. Also, the peaks of TiO₂ appeared at 2θ of 25.5°, and 38.2°, 39.5°, 47.3°, and 54.1°, which were related to anatase phases of TiO₂. This confirms that high coating and well dispersion of TiO₂ occurred on the surface of NaY-zeolite (42,43).

FT-IR analysis

The Fourier transform infrared spectroscopy (FT-IR)

spectra of the single NaY-zeolite, and TiO₂, and T/N-Z nanocomposite are presented in Figure 4a-c. According to Figure 4a, the FT-IR spectra of NaY-zeolite, the absorption peaks at wavenumbers of 435.62 and 1014.62 cm⁻¹ confirm the presence of the Si-O group in the nanocomposite structure. Also, the absorption peaks at wavenumbers of 540.10 cm⁻¹ was related to the Si-O-Al band. In Figure 4b, the absorption peaks at wavenumbers of 600 to 1000 cm⁻¹ was related to Ti-O-Ti bands (40,44). Also, a peak appeared at wavenumbers of 1600 and 3500 cm⁻¹ was related to the OH stretching of water (H₂O) or hydroxyl groups on the surface of TiO₂, which has a very important role in the photocatalytic reaction (32,45,46). In Figure 4c, the FTIR spectra of T/N-Z nanocomposite indicated that the absorption vibration peaks at wavenumbers of 438 and 1038 cm⁻¹ was related to the Si-O group. The FTIR spectrum at 900 cm⁻¹ to 960 cm⁻¹ is the characteristic peak of Ti-O-Si or Ti-O-Al vibration (47,48). Finally, the results demonstrated that the heterogeneous structure of the T/N-Z nanocomposite was formed after the hydrothermal process.

Analysis of variance and model fitting

The effects of variables pH, contact time, and catalyst dose on the MC-LR removal are presented in Table 5. As shown in this table, the F-value of the quadratic model was 80.78, indicating that the model was significant. Also, if the value of "Prob>F" for each parameter is less than 0.05, the effect of this parameter on the MC-LR removal is significant. Therefore, the single parameters A, B, C have significant effects on the MC-LR removal. According to Table 4, the interactions of AB, AC, and BC, A², B², and C² is no significant interaction effect on the MC-LR removal ($P > 0.05$). So, the effect of other quadratic forms was not significant and could be removed from the final equation. The F-value associated with the lack of fit in this model was 3.48, indicating that the lack of fit was not significant. This means that the model fitted well ($P > 0.05$) with the experimental data and errors of the experiments are low.

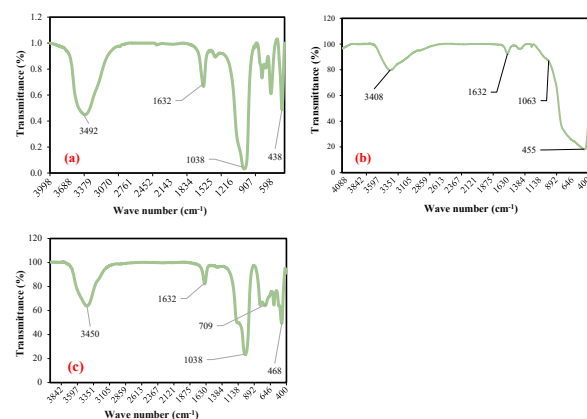


Figure 4. View of T/N-Z nanocomposite: SEM (a), FTIR (b), and XRD (c).

Table 5. Experimental design conditions and responses of various experimental runs

Source	Sum of squares	df	Mean square	F-value	P value Prob > F
Model	518.79	9	518.79	43.51	<0.0001
A: pH	289.13	1	289.13	218.21	<0.0001
B: Contact time	64.06	1	64.06	48.35	<0.0001
C: Catalyst dose	146.59	1	146.59	110.63	<0.0001
AB	5.54	1	5.54	4.18	0.0680
AC	1.08	1	1.08	0.82	0.3878
BC	0.64	1	0.64	0.48	0.5034
A ²	3.27	1	3.27	2.47	0.1473
B ²	5.91	1	5.91	4.46	0.0609
C ²	2.57	1	2.57	1.94	0.1936
Residual	13.25	10	1.32		
Lack of Fit	10.29	5	2.06	3.48	0.0987*
Pure Error	2.96	5	0.59		
Cor. Total	532.04	19			

Standard deviation: 1.15; Mean: 87.27; CV (%): 1.32; PRESS: 81.82; R²: 0.9751; Adjusted R²: 0.9527; Predicted R²: 0.8462; Adequate Precision: 25.643. *Not significant.

The values of R² and adjusted R² were obtained to be 0.9751 and 0.9527, respectively, indicating that the results of the model were fitted with experimental data. Finally, these relationships show that this model was significant. To survey the composed effect of the variables, all of the experiments were carried out with various combinations of the variables, which were statistically designed according to the CCD. To access a final model with significant predictors, the variables that had no significant ($P > 0.05$) interaction were eliminated from the model. Thus, other significant variables were retained in the final regression model. So, the following equation as the final equation was derived using the coefficient of the coded variables for removal of MC-LR (Eq. 4):

$$\text{Removal of MC-LR (\%)} = 88.39 - 4.78 A + 2.25 B + 3.40 C \quad (4)$$

The correlation between actual, predicted, and normal graphs of the residual related to the experimental data in removal of MC-LR is presented in Figures 5a and b. In these figures, data distribution was as a straight line, indicating that the experimental data were correlated by the predicted values of the response.

Discussion

Effect of variables on removal of MC-LR

Effect of single factors

Analysis of variance (ANOVA) for removal of MC-LR is presented in Table 4. Among pH, contact time, and catalyst dose as single variables, each factor with a high mean square and high F-value has the highest effect on the photodegradation of MC-LR by T/N-Z nanocomposite. So that, the effect of variables on the degradation of MC-

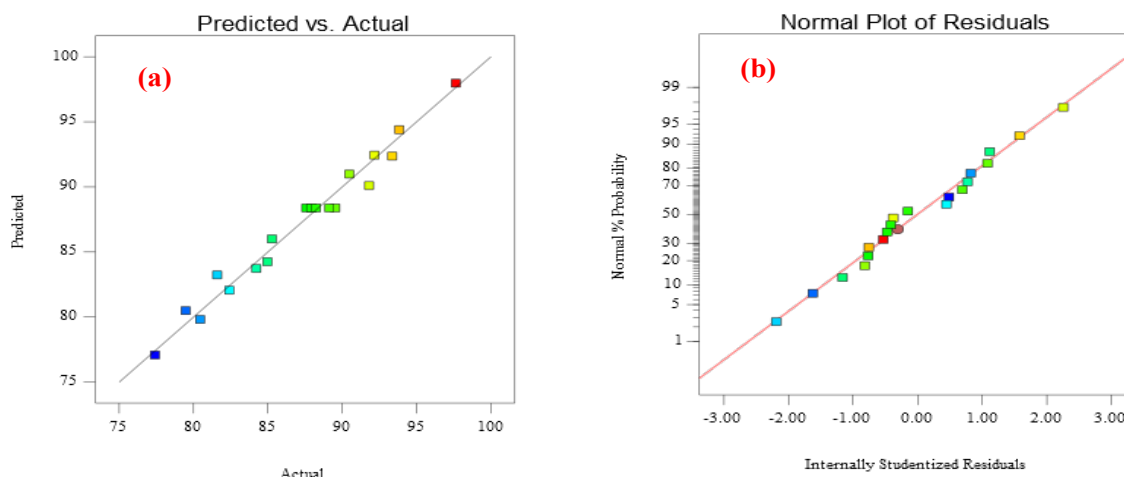


Figure 5. Model evaluation plots for removal of MC-LR by TiO₂: The experimental data vs. the predicted value plot (a); the normalized residual plot (b).

LR is as follows:

pH > Catalyst dose > Contact time

So, pH with mean square and F-value of 289.13 and 218.21, respectively, was the most important parameters in the MC-LR removal. These results were confirmed by the Pareto chart (Figure 6).

Effect of pH

The effect of various ranges of pH on the photocatalytic degradation of MC-LR is presented in Figure 7a. According to this figure, pH had a negative effect on the MC-LR removal, which was confirmed by the Pareto chart (Figure 6). So the rate of MC-LR degradation increased with the reduction of pH. Therefore, the MC-LR removal increased in the acidic pH range. According to the results of studies, in photocatalytic systems, the acidic pH range due to the strong electrostatic adsorption between the positive charge of catalyst and negative charge of the toxin was determined as the optimal pH in the photocatalytic degradation of toxins. So, the attractive forces between the catalyst and MC-LR molecules enhance the rate of MC-LR photodegradation (27). The pH_{pzc} of the synthesized nanocomposite in the present study was obtained to be 5.5. So, at pH values lower than pH_{pzc} , the surface charge of the catalyst would be positive and tended to absorb the negative charge of MC-LR. The study of Ebrahimi et al showed that the rate of MC-LR degradation increased to 93% at a pH of 5 (49). Liao et al reported that the photocatalytic degradation of MC-LR with Ag/AgCl/TiO₂ composite was increased by decreasing the initial pH, because of the effect of the attractive forces between the catalyst particles and toxin molecules (23). Also, the other similar study showed that the removal efficiency of Direct Red 16 was decreased at alkaline pH. Because, at acidic pH, with the occurrences of the electrostatic force interactions between dye molecules and the surface of the catalyst, photocatalytic activity was improved (46).

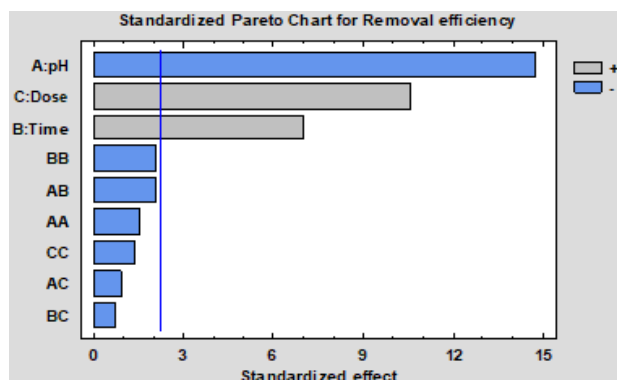


Figure 6. The standardized Pareto chart showing the effect of all factors on the MC-LR removal.

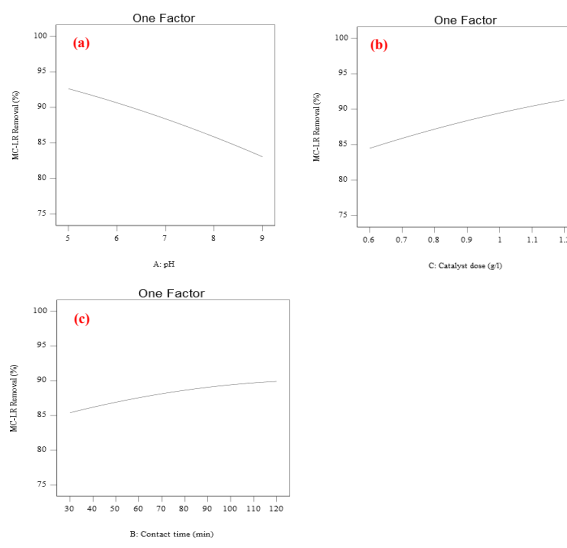


Figure 7. Effect of pH (a), catalyst dose (b), and contact time (c) on the MC-LR degradation (%).

Effect of catalyst dose

The effect of the T/N-Z nanocomposite dose on the MC-LR removal efficiency is presented in Figure 7b. As shown in this figure, the rate of MC-LR degradation is increasing with increasing the T/N-Z nanocomposite dose. The reason can be relevant to the enhancement of active sites on the surface of catalysts to capture more photons, which in turn leads to the generation of more hydroxyl and superoxide radicals, and finally, absorbance of more MC-LR molecules. Zhang et al reported that the rate of MC-LR degradation was enhanced with an increase in the catalyst dose due to the enhancement of surface area of the catalyst (50). Also, Arabzadeh et al and Koh et al reported that the photodegradation rate of tartrazine and Methylene Blue, respectively, enhanced by increasing the catalyst dose. Because the increase of catalyst dose can enhance the photocatalytic active sites to absorb more photons, and subsequently, lead to the generation of more hydroxyl and superoxide radicals, and finally, the degradation of more pollutant molecules (51,52).

Effect of contact time

Figure 7c shows the effect of contact time on the removal efficiency of MC-LR using T/N-Z nanocomposite. The results demonstrated that there is a positive relationship between contact time and MC-LR degradation. So that, by increasing the contact time, the MC-LR removal efficiency also increased because by increasing the contact time, the reaction time was enhanced, and subsequently, the probability of the interaction among MC-LR and the electron-hole pair increased. Rahimi et al showed that the rate of Acid Orange 10 dye degradation increased when the contact time increased, so that, with increasing the contact time from the beginning of the process to 150 minutes, the removal efficiency was increased from 0%

to 94% (39). Nawaz et al reported that the photocatalytic degradation of MC-LR using graphene-TiO₂/sodium alginate aerogels composite was increased with increasing the irradiation time (9). Similar studies by Massoudinejad et al and Arabzadeh et al showed that with enhancing the contact time, the removal efficiency of Direct Blue 71 and tartrazine, respectively, was increased because by increasing the contact time, photocatalytic activities on the catalyst surface increased (51,53).

Interaction relationship between studied variables

The effects of interactions between different variables on the MC-LR degradation (%) by the three-dimensional (3-D) response surface plots obtained from the quadratic model are indicated in Figure 8a. This figure presents the 3-D response surface plot of the MC-LR removal efficiency in various contact times vs. pH. According to this figure, with reducing pH and increasing contact time, the MC-LR removal efficiency was increased. The effect of pH on the MC-LR removal efficiency shown in this figure is more evident than that of contact time. However, the ANOVA results showed that the *P* value of the interaction effect of the coefficients of the contact time vs. pH was not significant (*P*=0.0680). The interaction effect between catalyst dose and pH on the MC-LR degradation (%) is illustrated in Figure 8b. As shown in this figure, the increase of catalyst dose and reduction of pH increased the MC-LR removal efficiency. But, the ANOVA results indicated that the interaction effect of the coefficients of catalyst dose vs. pH was not significant (*P*=0.3878) and did not display any interaction effects. Figure 8c shows 3-D response surface plot of the catalyst dose and contact time in the MC-LR removal efficiency. According to this figure,

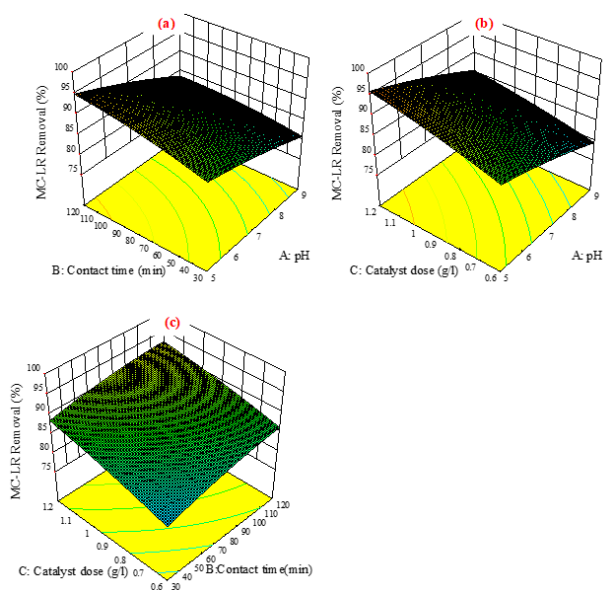


Figure 8. Interaction between different variables: (a) Contact time vs. initial pH; (b) catalyst dosage vs. initial pH; (c) catalyst dosage vs. contact time in the MC-LR degradation (%).

the catalyst dose and contact time had a positive effect on the removal efficiency of MC-LR. This means that the catalyst dose and contact time did not show interaction effects on the MC-LR removal. The ANOVA results approved that the interaction effect of the coefficients of these two parameters was not significant (*P*=0.5034).

Optimization of various process parameters

The optimum amounts of various variables including pH, contact time, and catalyst dose in the removal of MC-LR were optimized by the RSM model. The desirable goal in the RSM model was set on the maximum removal percentage of MC-LR. So, the optimum operating conditions of the synthesized TiO₂/NaY-zeolite nanocomposite in the removal of MC-LR are presented in Table 6. Finally, in order to estimate the validity of optimal conditions in the removal of MC-LR, three series of experiments were repeated with optimal conditions (97.35 ± 3.13). According to the results, there was a good agreement between these results and the predictions by Design Expert.

Possible photocatalytic mechanism and degradation pathway of MC-LR

Figure 9 illustrates the schematic diagram of MC-LR degradation mechanism by T/N-Z nanocomposite. As shown in this figure, the photodegradation reactions are occurring under ultraviolet (UV) light source as the following steps: Firstly, by irradiating UV light, a photon that has energy greater than or equal to the bandgap energy is absorbed by the photocatalyst, which excites an e⁻ to the CB of the catalyst, resulting in the generation of ·OH by the oxidation of water molecules with photogenerated holes and oxygenated species attacking the MC-LR molecules. In the next step, the e⁻ generated by photon absorption, reacts with oxygen absorbed on the catalyst surface and produces ·O₂⁻ radicals (39,40,46). According to the results of similar studies, the possible pathways of MC-LR degradation have been reported as follows: The hydroxyl radicals attack the C₄-C₅ and C₆-C₇ unsaturated double bonds in the Adda side-chain and diene bonds in the Adda chain or aromatic ring and result in the MC-LR hydroxylation (9,25). So that, the cleavage of double bonds in C₄-C₅ and C₆-C₇ resulted in the formation of aldehyde and ketone derivatives, respectively (25,54,55). Also, the cleavage of diene bonds in the Adda chain or aromatic ring

Table 6. Optimum conditions for removal of MC-LR

Factors	Units	Optimum values
pH	-	5
Contact time	min	120
Catalyst dose	g/L	1.2
Predicted removal efficiency	(%)	97.97
Actual removal efficiency	(%)	97.63

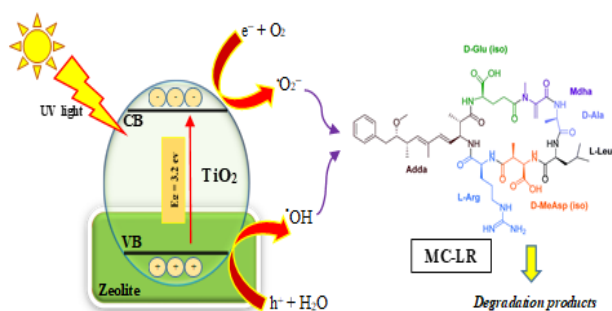
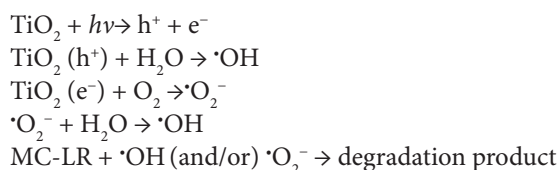


Figure 9. Schematic diagram of the MC-LR degradation mechanism.

can result in the production of intermediate products that were further oxidized and converted to aldehyde product (25,54). The main active radical in the oxidative process of MC-LR by TiO_2 (under UV light) is the $\cdot\text{OH}$ radical that has the ability to attack multiple positions on the MC-LR molecule. So that, the effect of $\cdot\text{O}_2^-$ radical on the removal of MC-LR is less than that of $\cdot\text{OH}$ radical (25). The role of zeolite as a facilitator in the degradation process, can bring MC-LR molecules closer to the catalyst surface and enhance the reaction rate of produced radicals with MC-LR, and even, in the combination with TiO_2 can prevent the recombination of e^-/h^+ pairs (39). Finally, the probable photochemical reactions in the MC-LR degradation by T/N-Z nanocomposite are presented as follows:



Evaluation of photocatalyst reusability

To investigate the reusability and stability of the T/N-Z nanocomposite, five recycling runs were performed for the MC-LR photocatalytic degradation (Figure 10). Because, the stability of the photocatalysts is one of the main advantages of their practical applications. According to Figure 10, the photocatalytic degradation of MC-LR was slightly decreased during five runs. So that, the removal efficiency of MC-LR from 96.88% in run 1 reached 89.64% in run 5. Therefore, in the trend of MC-LR photodegradation in the five runs, no significant change was observed in the photocatalytic activity of T/N-Z nanocomposite. So, the T/N-Z nanocomposite photocatalyst had a good stability during the photocatalytic degradation of MC-LR.

Conclusion

MC is a hepatotoxic and carcinogenic toxin that is generated by cyanotoxins, which can have adverse effects on the human health. Therefore, it is very important to remove it from the environment. In this study, T/N-Z

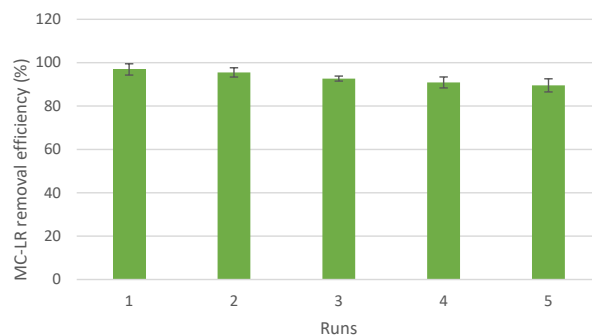


Figure 10. The reusability and stability of the T/N-Z nanocomposite in the MC-LR photocatalytic degradation.

nanocomposite was synthesized and optimized. Therefore, the effect of various variables including pH, contact time, and catalyst dose on the photocatalytic degradation of MC-LR was investigated using RSM methods based on the CCD design. The highest removal efficiency of MC-LR was observed at pH = 5. The results also showed that by increasing contact time and catalyst dose, the MC-LR removal efficiency also increased. The maximum removal efficiency of MC-LR (97.63%) was observed under optimal conditions (pH = 5, contact time = 120 minutes, and catalyst dosage = 1.2 g/L). Comparison of the variables showed that the effect of variables on the degradation of MC-LR is as follows: pH > catalyst dose > contact time. So, pH with mean square and F-value of 289.13 and 218.21, respectively, was the most important variable in the removal of MC-LR. In general, T/N-Z nanocomposite in aqueous solutions under the UV light can easily degrade MC-LR and it can also be proposed as an effective composite for the photocatalytic degradation of MC-LR.

Acknowledgements

This study is a part of a Ph.D. approved thesis (No. 395847), which was performed at Isfahan University of Medical Sciences, Isfahan, Iran. The authors would like to gratitude Department of Environmental Health Engineering and Environment Research Center, Isfahan University of Medical Sciences, Isfahan, for its financial support.

Ethical issues

The authors certify that this manuscript is the original work of the authors, and all data collected during the study are presented in this manuscript, and no data from the study has been or will be published separately (Ethical code: R.MUI.REC.1395.3.847).

Competing interests

Authors declare that they have no conflict of interests.

Authors' contributions

All authors contributed equally and participated in the data collection, analysis, and interpretation. All authors

critically reviewed, refined, and approved the manuscript.

References

1. Sukenik A, Quesada A, Salmaso N. Global expansion of toxic and non-toxic cyanobacteria: effect on ecosystem functioning. *Biodivers Conserv* 2015; 24(4): 889-908. doi: 10.1007/s10531-015-0905-9.
2. Dittmann E, Wiegand C. Cyanobacterial toxins--occurrence, biosynthesis and impact on human affairs. *Mol Nutr Food Res* 2006; 50(1): 7-17. doi: 10.1002/mnfr.200500162.
3. Mohamed ZA, Hashem M, Alamri S, Mostafa Y. Cyanotoxins and their environmental health risk in marine and freshwaters of Saudi Arabia. *Arab J Geosci* 2020; 13(7): 285. doi: 10.1007/s12517-020-5238-7.
4. Merel S, Walker D, Chicana R, Snyder S, Baurès E, Thomas O. State of knowledge and concerns on cyanobacterial blooms and cyanotoxins. *Environ Int* 2013; 59: 303-27. doi: 10.1016/j.envint.2013.06.013.
5. Zhao CS, Shao NF, Yang ST, Ren H, Ge YR, Feng P, et al. Predicting cyanobacteria bloom occurrence in lakes and reservoirs before blooms occur. *Sci Total Environ* 2019; 670: 837-48. doi: 10.1016/j.scitotenv.2019.03.161.
6. Yang F, Huang F, Feng H, Wei J, Massey IY, Liang G, et al. A complete route for biodegradation of potentially carcinogenic cyanotoxin microcystin-LR in a novel indigenous bacterium. *Water Res* 2020; 174: 115638. doi: 10.1016/j.watres.2020.115638.
7. Lundqvist J, Pekar H, Oskarsson A. Microcystins activate nuclear factor erythroid 2-related factor 2 (Nrf2) in human liver cells in vitro - implications for an oxidative stress induction by microcystins. *Toxicol* 2017; 126: 47-50. doi: 10.1016/j.toxicol.2016.12.012.
8. Kelly NE, Javed A, Shimoda Y, Zastepa A, Watson S, Mugalingam S, et al. A Bayesian risk assessment framework for microcystin violations of drinking water and recreational standards in the Bay of Quinte, Lake Ontario, Canada. *Water Research* 2019; 162: 288-301. doi: 10.1016/j.watres.2019.06.005.
9. Nawaz M, Moztahida M, Kim J, Shahzad A, Jang J, Miran W, et al. Photodegradation of microcystin-LR using graphene-TiO₂/sodium alginate aerogels. *Carbohydr Polym* 2018; 199: 109-18. doi: 10.1016/j.carbpol.2018.07.007.
10. Zewde TW, Johansen JA, Kifle D, Demissie TB, Hansen JH, Tadesse Z. Concentrations of microcystins in the muscle and liver tissues of fish species from Koka reservoir, Ethiopia: a potential threat to public health. *Toxicol* 2018; 153: 85-95. doi: 10.1016/j.toxicol.2018.08.013.
11. Henao E, Rzymiski P, Waters MN. A review on the study of cyanotoxins in paleolimnological research: current knowledge and future needs. *Toxins (Basel)* 2019; 12(1). doi: 10.3390/toxins12010006.
12. Zhang G, Zhang YC, Nadagouda M, Han C, O'Shea K, El-Sheikh SM, et al. Visible light-sensitized S, N and C co-doped polymorphic TiO₂ for photocatalytic destruction of microcystin-LR. *Appl Catal B Environ* 2014; 144: 614-21. doi: 10.1016/j.apcatb.2013.07.058.
13. Liu B, Qu F, Chen W, Liang H, Wang T, Cheng X, et al. *Microcystis aeruginosa*-laden water treatment using enhanced coagulation by persulfate/Fe(II), ozone and permanganate: Comparison of the simultaneous and successive oxidant dosing strategy. *Water Res* 2017; 125: 72-80. doi: 10.1016/j.watres.2017.08.035.
14. Sun J, Bu L, Deng L, Shi Z, Zhou S. Removal of *Microcystis aeruginosa* by UV/chlorine process: inactivation mechanism and microcystins degradation. *Chem Eng J* 2018; 349: 408-15. doi: 10.1016/j.cej.2018.05.116.
15. Wu P, Li G, He Y, Luo D, Li L, Guo J, et al. High-efficient and sustainable biodegradation of microcystin-LR using *Sphingopyxis* sp. YF1 immobilized Fe₃O₄@chitosan. *Colloids Surf B Biointerfaces* 2020; 185: 110633. doi: 10.1016/j.colsurfb.2019.110633.
16. Liu G, Zhang G, Zhang S, Xu Y, Yang X, Zhang X. Degradation and mechanism of microcystin-LR by PbCrO₄ nanorods driven by visible light. *Chemosphere* 2020; 239: 124739. doi: 10.1016/j.chemosphere.2019.124739.
17. Pham TL, Dang TN. Microcystins in freshwater ecosystems: occurrence, distribution, and current treatment approaches. In: Bui XT, Chiemchaisri C, Fujioka T, Varjani S, eds. *Water and Wastewater Treatment Technologies*. Singapore: Springer; 2019. p. 15-36. doi: 10.1007/978-981-13-3259-3_2.
18. Park JA, Yang B, Jang M, Kim JH, Kim SB, Park HD, et al. Oxidation and molecular properties of microcystin-LR, microcystin-RR and anatoxin-a using UV-light-emitting diodes at 255 nm in combination with H₂O₂. *Chem Eng J* 2019; 366: 423-32. doi: 10.1016/j.cej.2019.02.101.
19. Liu Y, Ren J, Wang X, Fan Z. Mechanism and reaction pathways for microcystin-LR degradation through UV/H₂O₂ treatment. *PLoS One* 2016; 11(6): e0156236. doi: 10.1371/journal.pone.0156236.
20. Pelaez M, de la Cruz AA, Stathatos E, Falaras P, Dionysiou DD. Visible light-activated N-F-codoped TiO₂ nanoparticles for the photocatalytic degradation of microcystin-LR in water. *Catal Today* 2009; 144(1-2): 19-25. doi: 10.1016/j.cattod.2008.12.022.
21. Yang B, Park HD, Hong SW, Lee SH, Park JA, Choi JW. Photocatalytic degradation of microcystin-LR and anatoxin-a with presence of natural organic matter using UV-light emitting diodes/TiO₂ process. *J Water Process Eng* 2020; 34: 101163. doi: 10.1016/j.jwpe.2020.101163.
22. Pestana CJ, Edwards C, Prabhu R, Robertson PKJ, Lawton LA. Photocatalytic degradation of eleven microcystin variants and nodularin by TiO₂ coated glass microspheres. *J Hazard Mater* 2015; 300: 347-53. doi: 10.1016/j.jhazmat.2015.07.016.
23. Liao W, Zhang Y, Zhang M, Murugananthan M, Yoshihara S. Photoelectrocatalytic degradation of microcystin-LR using Ag/AgCl/TiO₂ nanotube arrays electrode under visible light irradiation. *Chem Eng J* 2013; 231: 455-63. doi: 10.1016/j.cej.2013.07.054.
24. Qi K, Cheng B, Yu J, Ho W. A review on TiO₂-based Z-scheme photocatalysts. *Chinese J Catal* 2017; 38(12): 1936-55. doi: 10.1016/s1872-2067(17)62962-0.
25. Hu X, Hu X, Tang C, Wen S, Wu X, Long J, et al. Mechanisms underlying degradation pathways of microcystin-LR with doped TiO₂ photocatalysis. *Chem Eng J* 2017; 330: 355-71. doi: 10.1016/j.cej.2017.07.161.
26. Diaz-Angulo J, Lara-Ramos J, Mueses M, Hernández-Ramírez A, Li Puma G, Machuca-Martínez F. Enhancement of the oxidative removal of diclofenac and of the TiO₂ rate of photon absorption in dye-sensitized solar pilot scale CPC

- photocatalytic reactors. *Chem Eng J* 2020; 381: 122520. doi: 10.1016/j.cej.2019.122520.
27. Jafari N, Ebrahimpour K, Abdollahnejad A, Karimi M, Ebrahimi A. Efficient degradation of microcystin-LR by BiVO₄/TiO₂ photocatalytic nanocomposite under visible light. *J Environ Health Sci Eng* 2019; 17(2): 1171-83. doi: 10.1007/s40201-019-00432-4.
 28. Liu X, Liu Y, Lu S, Guo W, Xi B. Performance and mechanism into TiO₂/Zeolite composites for sulfadiazine adsorption and photodegradation. *Chem Eng J* 2018; 350: 131-47. doi: 10.1016/j.cej.2018.05.141.
 29. Qileng A, Cai Y, Wei J, Lei H, Liu W, Zhang S, et al. Construction of CdS/B-TiO₂ nanorods photoelectrochemical immunosensor for the detection of microcystin-LR using SiO₂@G-quadruplex as multi-amplifier. *Sens Actuators B Chem* 2018; 254: 727-35. doi: 10.1016/j.snb.2017.07.164.
 30. Yang J, Chen DX, Deng AP, Huang YP, Chen CC. Visible-light-driven photocatalytic degradation of microcystin-LR by Bi-doped TiO₂. *Res Chem Intermed* 2011; 37(1): 47-60. doi: 10.1007/s11164-010-0224-4.
 31. Wang SL, Wang LL, Ma WH, Johnson DM, Fang YF, Jia MK, et al. Moderate valence band of bismuth oxyhalides (BiOXs, X=Cl, Br, I) for the best photocatalytic degradation efficiency of MC-LR. *Chem Eng J* 2015; 259: 410-6. doi: 10.1016/j.cej.2014.07.103.
 32. Farhadi N, Tabatabaie T, Ramavandi B, Amiri F. Optimization and characterization of zeolite-titanate for ibuprofen elimination by sonication/hydrogen peroxide/ultraviolet activity. *Ultrason Sonochem* 2020; 67: 105122. doi: 10.1016/j.ultsonch.2020.105122.
 33. Suárez S, Jansson I, Ohtani B, Sánchez B. From titania nanoparticles to decahedral anatase particles: Photocatalytic activity of TiO₂/zeolite hybrids for VOCs oxidation. *Catal Today* 2019; 326: 2-7. doi: 10.1016/j.cattod.2018.09.004.
 34. Naghdali Z, Sahebi S, Ghanbari R, Mousazadeh M, Ali Jamali H. Chromium removal and water recycling from electroplating wastewater through direct osmosis: modeling and optimization by response surface methodology. *Environ Health Eng Manag* 2019; 6(2): 113-20. doi: 10.15171/ehem.2019.13.
 35. Wei X, Xu X, Yang X, Li J, Liu Z. Visible light degradation of reactive black-42 by novel Sr/Ag-TiO₂@g-C₃N₄ photocatalyst: RSM optimization, reaction kinetics and pathways. *Spectrochim Acta A Mol Biomol Spectrosc* 2020; 228: 117870. doi: 10.1016/j.saa.2019.117870.
 36. Nikazar M, Gholivand K, Mahanpoor K. Photocatalytic degradation of azo dye Acid Red 114 in water with TiO₂ supported on clinoptilolite as a catalyst. *Desalination* 2008; 219(1-3): 293-300. doi: 10.1016/j.desal.2007.02.035.
 37. Faraji M, Ebrahimi A, Nourmoradi H, Nikoonahad A, Abdollahnejad A, Ghanbari R, et al. Optimizing the removal of humic acid with polyaluminum chloride and polyaluminum ferric chloride as green coagulants using response surface methodology. *Desalin Water Treat* 2019; 139:297-304. doi: 10.5004/dwt.2019.23309.
 38. Mohammadi A, Nemati S, Mosafieri M, Abdollahnejad A, Almasian M, Sheikhmohammadi A. Predicting the capability of carboxymethyl cellulose-stabilized iron nanoparticles for the remediation of arsenite from water using the response surface methodology (RSM) model: modeling and optimization. *J Contam Hydrol* 2017; 203: 85-92. doi: 10.1016/j.jconhyd.2017.06.005.
 39. Rahimi B, Jafari N, Abdollahnejad A, Farrokhzadeh H, Ebrahimi A. Application of efficient photocatalytic process using a novel BiVO₄/TiO₂-NaY zeolite composite for removal of acid orange 10 dye in aqueous solutions: Modeling by response surface methodology (RSM). *J Environ Chem Eng* 2019; 7(4): 103253. doi: 10.1016/j.jece.2019.103253.
 40. Rahimi B, Ebrahimi A. Photocatalytic process for total arsenic removal using an innovative BiVO₄/TiO₂/LED system from aqueous solution: optimization by response surface methodology (RSM). *J Taiwan Inst Chem Eng* 2019; 101: 64-79. doi: 10.1016/j.jtice.2019.04.036.
 41. Hu J, Jiang N, Li J, Shang K, Lu N, Wu Y. Degradation of benzene by bipolar pulsed series surface/packed-bed discharge reactor over MnO₂-TiO₂/zeolite catalyst. *Chem Eng J* 2016; 293: 216-24. doi: 10.1016/j.cej.2016.02.036.
 42. Ling C, Yue C, Yuan R, Qiu J, Liu FQ, Zhu JJ. Enhanced removal of sulfamethoxazole by a novel composite of TiO₂ nanocrystals in situ wrapped-Bi₂O₄ microrods under simulated solar irradiation. *Chem Eng J* 2020; 384: 123278. doi: 10.1016/j.cej.2019.123278.
 43. Derakhshan-Nejad A, Rangkooy HA, Cheraghi M, Yengejeh RJ. Removal of ethyl benzene vapor pollutant from the air using TiO₂ nanoparticles immobilized on the ZSM-5 zeolite under UVradiation in lab scale. *J Environ Health Sci Eng* 2020; 18(1): 201-9. doi: 10.1007/s40201-020-00453-4.
 44. Li H, Cui X. A hydrothermal route for constructing reduced graphene oxide/TiO₂ nanocomposites: enhanced photocatalytic activity for hydrogen evolution. *Int J Hydrogen Energy* 2014; 39(35): 19877-86. doi: 10.1016/j.ijhydene.2014.10.010.
 45. Rafiee E, Noori E, Zinatizadeh AA, Zanganeh H. A new visible driven nanocomposite including Ti-substituted polyoxometalate/TiO₂: synthesis, characterization, photodegradation of azo dye process optimization by RSM and specific removal rate calculations. *J Mater Sci Mater Electron* 2018; 29(24): 20668-79. doi: 10.1007/s10854-018-0205-8.
 46. Zanganeh H, Farhadian M, Zinatizadeh AA. N (Urea) and CN (L-Asparagine) doped TiO₂-CuO nanocomposites: fabrication, characterization and photodegradation of direct red 16. *J Environ Chem Eng* 2020; 8(1): 103639. doi: 10.1016/j.jece.2019.103639.
 47. Faghian H, Bahranifard A. Application of TiO₂-zeolite as photocatalyst for photodegradation of some organic pollutants. *Iran J Catal* 2011; 1(1): 45-50.
 48. Nagarjuna R, Challagulla S, Alla N, Ganesan R, Roy S. Synthesis and characterization of reduced-graphene oxide/TiO₂/Zeolite-4A: a bifunctional nanocomposite for abatement of methylene blue. *Mater Des* 2015; 86: 621-6. doi: 10.1016/j.matdes.2015.07.116.
 49. Ebrahimi A, Ebrahim K, Abdollahnejad A, Jafari N, Karimi M, Mohammadi A, et al. Photocatalytic degradation of microcystin-LR using BiVO₄ photocatalysts under visible light irradiation: modelling by response surface methodology (RSM). *Int J Environ Anal Chem* 2020; 1-18. doi: 10.1080/03067319.2020.1820498.
 50. Zhang H, Zhu G, Jia X, Ding Y, Zhang M, Gao Q, et al. Removal of microcystin-LR from drinking water using a bamboo-based charcoal adsorbent modified with chitosan.

- J Environ Sci 2011; 23(12): 1983-8. doi: 10.1016/s1001-0742(10)60676-6.
51. Arabzadeh N, Mohammadi A, Darwish M, Abuzerr S. Construction of a TiO₂-Fe₃O₄-decorated molecularly imprinted polymer nanocomposite for tartrazine degradation: response surface methodology modeling and optimization. J Chin Chem Soc 2019; 66(5): 474-83. doi: 10.1002/jccs.201800302.
52. Koh PW, Yuliati L, Lee SL. Kinetics and optimization studies of photocatalytic degradation of methylene blue over Cr-doped TiO₂ using response surface methodology. Iran J Sci Technol Trans A Sci 2019; 43(1): 95-103. doi: 10.1007/s40995-017-0407-6.
53. Massoudinejad M, Sadani M, Gholami Z, Rahmati Z, Javaheri M, Keramati H, et al. Optimization and modeling of photocatalytic degradation of Direct Blue 71 from contaminated water by TiO₂ nanoparticles: response surface methodology approach (RSM). Iran J Catal 2019; 9(2): 121-32.
54. Andersen J, Han C, O'Shea K, Dionysiou DD. Revealing the degradation intermediates and pathways of visible light-induced NF-TiO₂ photocatalysis of microcystin-LR. Appl Catal B Environ 2014; 154-155: 259-66. doi: 10.1016/j.apcatb.2014.02.025.
55. Wang X, Wang X, Zhao J, Song J, Zhou L, Wang J, et al. An alternative to in situ photocatalytic degradation of microcystin-LR by worm-like N, P co-doped TiO₂/expanded graphite by carbon layer (NPT-EGC) floating composites. Appl Catal B Environ 2017; 206: 479-89. doi: 10.1016/j.apcatb.2017.01.046.